COMMUNICATIONS IN SCIENCE AND TECHNOLOGY
Homepage: cst.kipmi.or.id

Eco-friendly synthesis of magnetite based on tea dregs (Fe_3O_4-TD) for methylene blue adsorbent from simulation waste

Maya Rahmayanti*, Atika Yahdiyani, Ika Qurrotul Afifah

Chemistry Department, UIN Sunan Kalijaga Yogyakarta, Yogyakarta 55281, Indonesia

Article history:
Received: 17 September 2022 / Received in revised form: 5 November 2022 / Accepted: 10 November 2022

Abstract

Methylene blue is a popular dye used in the batik industry; however, it potentially causes environmental problems in view of the residual MB content in the liquid waste, which is difficult to naturally degrade. This study aims to synthesize Fe_3O_4-TD using tea dregs from household waste and its application as an adsorbent for methylene blue dye. The synthesis was carried out using the reverse co-precipitation method with water as a solvent at room temperature. Fe_3O_4-TD was characterized using FTIR, XRD, and PSA. The adsorption of methylene blue (MB) on Fe_3O_4-TD was studied at various pH, reaction time, and concentration to determine the kinetic model and MB adsorption isotherm on Fe_3O_4-TD and the interactions occurred between MB and Fe_3O_4-TD. FTIR spectra and X-Ray diffractogram showed that the magnetite formed in a pure state was not mixed with other iron oxides. The crystal and particle size of Fe_3O_4-TD was 18.92 nm and 26.70 µm, respectively. MB adsorption on Fe_3O_4-TD occurred at pH > 3 and followed Ho's pseudo-second-order kinetics model and the Freundlich isotherm model. The rate constants (k) and the initial adsorption rate (h) of MB adsorption on Fe_3O_4-TD were 5.0 x 10^{-4} g/mg.minute and 5.0 x 10^4 mg/g.minute. Meanwhile, the amount of MB adsorbed at equilibrium (q_e) was 1.0 x 10^4 mg/g and the maximum adsorption capacity of MB on Fe_3O_4-TD was 10.21 mol/g. The MB and Fe_3O_4-TD interacted through electrostatic interactions, hydrogen bonds, and π-π interactions.

Keywords: Magnetite; tea dregs; methylene blue; adsorption; dye

1. Introduction

Methylene blue is a synthetic dye widely used in the batik industry considering its advantage to make the batik color sharper, brighter, and longer-lasting. About 45% of the dye is attached to the batik cloth in the dyeing process, and the rest is decolorized in the washing process [1]. Liquid waste that contains dye from the washing process, however, potentially causes environmental problems because synthetic dyes are non-biodegradable, toxic, and highly soluble [2].

Various studies related to the synthetic dye processing have been carried out, including regarding the ozonation method [3], coagulation and flocculation [4], biological treatment using bacteria [5], electrochemistry [6], and oxidation [7]. However, some weaknesses in these studies are found still. Ozonization and electrochemical methods are unfavorable to apply in batik industry considering the high costs. Coagulation and filtration methods produce a new problem in the form of sludge in relatively large quantities. Also, biological treatment is often ineffective because bacteria are unable to adapt to the dye's complexity. The adsorption method is eloquently suitable to treat dye waste as it is a low-cost and fast process to apply with simple equipment in the batik industry. However, producing waste in the form of adsorbents that have bound dyes has led to new issues. Despite the production of adsorbent waste, it can be regenerated by carrying out the desorption process so that the adsorbent and adsorbate can be reused. The selection of stable, inexpensive, and easy-to-synthesize regenerated adsorbents is foremost to be investigated.

In recent years, magnetic adsorbents have been developed [1,10,18]. They can facilitate the separation process between the post-adsorption adsorbent and the filtrate using an external magnetic field to minimize the use of filter paper and save separation time [1,8,16]. The most widely developed magnetic compound is magnetite (Fe_3O_4) because of its stability and paramagnetic properties.

This research synthesized magnetite (Fe_3O_4) adsorbent based on tea dregs waste from household waste. Tea dregs contain secondary metabolites that are phenolic compounds, such as catechins, i.e. flavonoids, flavanols, and polyphenols [20,28]. It also contains cellulose, hemicellulose, lignin, and a little protein. The presence of phenolic compounds in tea dregs and solubility in water provokes the action as a reducing agent and a capping agent in synthesizing Fe_3O_4. In addition, organic compounds are reported to have hydrophobic properties and steric barrier effects enabling them to control particle growth and prevent agglomeration during Fe_3O_4 synthesis [8]. The hydroxy group contained in tea dregs can also enrich the active site of Fe_3O_4-TD particles to increase the ability of Fe_3O_4-TD as an adsorbent. In addition, the utilization of tea dregs is an

* Corresponding author.
Email: maya.rahmayanti@uin-suka.ac.id
hhttps://doi.org/10.21924/cst.7.2.2022.965

exciting thing to study because it can help to overcome environmental pollution. Tea dregs waste discharged into the environment without processing will be able to pollute the environment. In fact, it becomes one of the household wastes produced every day.

The magnetic properties of Fe_3O_4-TD cause Fe_3O_4-TD adsorbent to be easily regenerated. In addition, the adsorption process can be carried out more easily and quickly with the help of an external magnetic field. Costs can be diminished for requiring no filter paper to separate the adsorbent and filtrate. The straightforward process will cut off the long time to complete the filtration process.

In this study, the synthesis of Fe_3O_4-TD was carried out by the reverse co-precipitation method and applied as an adsorbent of methylene blue (MB). The effects of pH dye on MB adsorption on Fe_3O_4-TD were studied at various pH ranges. In addition, MB adsorption kinetics and isotherms on Fe_3O_4-TD were also studied.

2. Materials and Methods

The materials used in this study were purchased from Merck Co. (proanalytical grade), including iron (II) sulfate heptahydrate ($FeSO_4 \cdot 7H_2O$) and iron(III)chloride hexahydrate ($FeCl_3 \cdot 6H_2O$), sodium hydroxide (NaOH), and methylene blue. The solvent used for the material preparation stage was aquabidest from PT. Ikapharmindo Putramas, while the dye solvent used aquadest. Meanwhile, tea dregs were obtained from household waste.

2.1. Preparation of tea dregs extract (TDE)

The tea dregs from household waste were dried using an oven at 60°C for 2 hours. Dried tea dregs were then mashed using a blender. The extract was prepared by heating 10 g of tea dregs with 100 mL of aquabidest solvent at 60°C for 20 minutes. Next, the mixture was filtered using Whatman paper No. 1. The filtrate subsequently was stored in the refrigerator before being used in the next step.

2.2. Preparation of Fe_3O_4-TD

Fe_3O_4-TD preparation was conducted by making a solution of Fe^{3+}, Fe^{2+}, and NaOH. Fe^{3+} and Fe^{2+} solutions (molar ratio Fe^{3+}/Fe^{2+}=2:1) were prepared by dissolving 0.556 g $FeCl_3 \cdot 6H_2O$ and 1.082 g $FeSO_4 \cdot 7H_2O$ in 50 mL of distilled water. NaOH 1 M solution, meanwhile, was prepared by dissolving 0.8 g of solid NaOH into 20 mL of distilled water. Furthermore, Fe^{3+} and Fe^{2+} were mixed before being slowly dropped into the NaOH solution. After all, the Fe^{3+} and Fe^{2+} solutions were dripped, 15 mL of tea dreg extract, cooled at room temperature, was poured quickly into the solution. Furthermore, stirring was carried out for 60 minutes at room temperature. The precipitate formed was decanted using an external magnetic field and dried in an oven at 60°C for 60 minutes.

2.3. Characterization of Fe_3O_4-TD

Fe_3O_4-TD was characterized using several instruments, such as the FTIR Spectrophotometer (Nicolet Avatar 360 IR) in the transmission mode using the KBr method for all powders and X-Rays diffraction pattern (XRD) using a Bruker D2 diffractometer with Cu Ka radiation (λ = 0.1546 nm), and particle size analyzer (PSA) Horiba LA 350. Characterization using FTIR was to determine the content of functional groups and characterization using XRD was scanned in the two thetas (2θ) in the range of 25° to 65° with a count of 4 seconds per step. The crystallinity and size of the Fe_3O_4-TD were generated from the XRD diffractograms. Meanwhile, PSA characterization was to determine the particle size of Fe_3O_4-TD.

2.4. Methylene blue adsorption studies

The adsorption of methylene blue on Fe_3O_4-TD was carried out using the batch method with variations in the pH of the methylene blue solution, reaction time, and the concentration of methylene blue.

2.4.1. pH optimization of methylene blue

10 mg Fe_3O_4-TD was added to 25 mL of MB dye solution 15 ppm at various pHs 2, 4, 6, 8, and 10. The mixture was shaken using a shaker for 60 minutes at room temperature. Then, the residue and filtrate were separated using an external magnetic field. The MB concentration in the filtrate was analyzed using a UV-Vis spectrophotometer. The adsorbed MB concentration referred to the difference between the MB concentration in the control solution and the remaining MB concentration in the filtrate.

2.4.2. Time optimization and adsorption kinetics studies

10 mg Fe_3O_4-TD was added to 25 mL of MB dye solution with optimum pH, and the mixture was shaken using a shaker at room temperature with time variations of 15, 30, 60, 90, and 120 minutes. The residue and filtrate were separated using an external magnetic field. The MB concentration in the filtrate was analyzed using a UV-Vis spectrophotometer. The adsorbed MB concentration was the difference between the MB concentration in the control solution and the remaining MB concentration in the filtrate. The optimum time for MB adsorption on Fe_3O_4-TD was obtained based on the highest % of MB adsorbed. The adsorption kinetics models of MB onto Fe_3O_4-TD studied in this study were Lagergren's pseudo-first-order kinetics model and Ho's pseudo-second-order kinetics model.

2.5.3. Adsorption isotherm study

MB adsorption isotherm model on Fe_3O_4-TD was studied using Langmuir and Freundlich isotherm model. A total of 10 mg of Fe_3O_4-TD was added to 25 mL of MB solution with various concentrations of 5, 10, 15, 20, and 25 ppm. The reaction was carried out at the optimum pH and time. The precipitate and filtrate were separated using an external magnetic field. MB remaining in each solution was determined using a UV-Vis spectrophotometer.

3. Results and Discussion

3.1. Characterization of Fe_3O_4-TD

Fe_3O_4-TD was synthesized using the reverse co-precipitation method with NaOH as the precipitating agent. The

concentration of NaOH solution was adjusted so that the pH of the reaction medium was above pH 12. The goal was that the resulting Fe_3O_4 did not mix with other iron oxides, such as hematite (Fe_2O_3) or goethite (FeOOH). According to the simplified pourbaix diagram, the iron-water system at 77°F (25°C), Fe_3O_4 and $Fe(OH)_2$ were stable at pH > 8, while Fe_2O_3 was stable at pH > 3. The characterization using FTIR and XRD spectrophotometers was essential to prove whether Fe_3O_4-TD was not mixed with $Fe(OH)_2$ and Fe_2O_3.

Figure 1 shows the spectra of Fe_3O_4, tea dregs, and Fe_3O_4-TD. In the Fe_3O_4 and Fe_3O_4-TD spectra, absorptions appeared in the area around 570 cm^{-1} and 410 cm^{-1}, typical absorptions for Fe-O bonds to Fe_3O_4. The structure of Fe_3O_4 had Fe^{3+} and Fe^{2+} ions and 32 oxygen ions. Fe^{3+} ions were located in the center of the tetrahedron for each part of the tetrahedral, and oxygen ions occupied the four corners. Meanwhile, Fe^{3+} and Fe^{2+} ions for the octahedral part were located in the middle of the octahedron, and the six corners were occupied by oxygen ions [9]. In the FTIR spectra, the stretching vibration of Fe-O was bound in the tetrahedral unit indicated by the appearance of absorption in the 570 cm^{-1} area. In contrast, the Fe-O strain vibration in the octahedral unit was characterized by the appearance of absorption in the area around 410 cm^{-1} [10-12]. The presence of two absorptions in this area in the Fe_3O_4 and Fe_3O_4-TD spectra indicated that Fe_3O_4 and Fe_3O_4-TD have been successfully synthesized. To determine whether Fe_3O_4 was not mixed with Fe_2O_3 and $Fe(OH)_2$, characterization was carried out using XRD. TD contains phenolic compounds such as catechins, a group of flavonoids, flavanols, and polyphenols [20,28]. The functional groups of these compounds were -OH groups, -CH alkanes, -CH aromatics, -C=O, and -C-O carboxylic acids. Figure 1 shows strong absorption in the 3400 cm^{-1} regions in both the TD and Fe_3O_4-TD spectra, which indicated the presence of a phenolic -OH group. The absorption at the wavenumber 2365 cm^{-1} indicated the presence of the C=C group. Meanwhile, the presence of aryl ketone groups was indicated by the appearance of absorption in the area around 1600 cm^{-1}. The absorptions in the Fe_3O_4-TD spectra were a combination of TD and Fe_3O_4 absorptions, indicating that Fe_3O_4-TD has been successfully synthesized. Fe^{2+} was very easily oxidized to Fe^{3+}, causing the molar ratio of $Fe^{3+}/Fe^{2+} \neq 2:1$. The abundant -OH group in tea dregs can act as a reducing agent that maintains the balance of the molar ratio of Fe^{3+} and Fe^{2+} in solution = 2:1 to produce magnetite (Fe_3O_4) with higher purity [8,12,17].

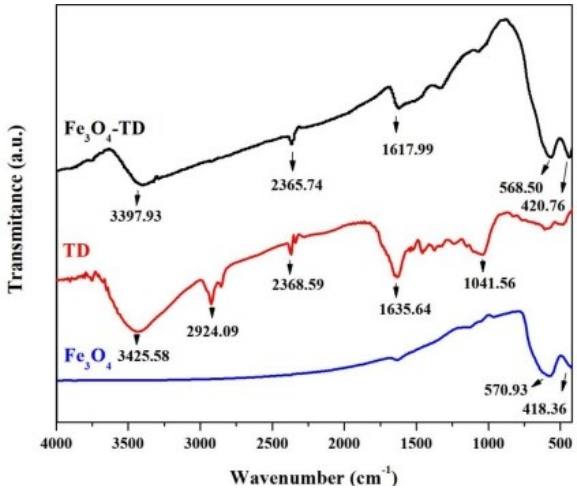

Fig. 1. FTIR spectra of pure Fe_3O_4, tea dregs, and Fe_3O_4-TD

Figure 2 shows the XRD Fe_3O_4-TD diffractogram. The peaks occurred at 2θ = 30.3°, 35.7°, 43.3°, 53.7°, 57.3°, and 62.9°, which could be indexed to (220), (311), (400), (422), (511), and (440) planes. This peak corresponded to the pure Fe_3O_4 peak, according to the Joint Committee on Powder Diffraction Standards (JCPDs No. 19-0629). The synthesized Fe_3O_4-TD did not mix with other iron oxides, such as Fe_2O_3. The magnetic properties of Fe_3O_4-TD are evidenced from Figure 3. Based on the XRD diffractogram, the average crystal size of Fe_3O_4-TD can be determined using Debye–Scherrer's equation based on full width at half maximum (FWHM = 0.461) of the (311) reflection. Table 1 presents the comparison of the crystal size of Fe_3O_4-TD with the crystal size of other magnetic particles. The crystal size determined the crystallinity of Fe_3O_4-TD. The smaller the crystal size, the better the crystallinity of the particles [13,14,15].

Table 1. Comparison of the crystal size of Fe_3O_4-TD with the crystal size of other magnetic particles

Plant extract	Synthesis condition	The average crystal size (nm)
Archidendron pauciflorum peel extract (JPE) [8]	pH 11–12, 60 min, 60 °C	17.6 - 20.90
Persicaria bistorta root extract [16]	pH 11, 120 min, 70 °C	47.0
Tea dregs extract (this study)	pH 11, 60 min, 60 °C	18.92
Fe_3O_4	pH 11, 60 min, 60 °C	14.99

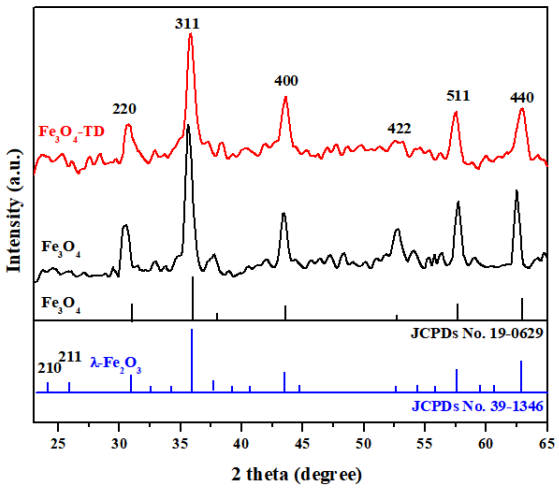

Fig. 2. XRD patterns of Fe_3O_4-TD

Fig. 3. Image of Fe_3O_4-TD attracted by an external magnetic field

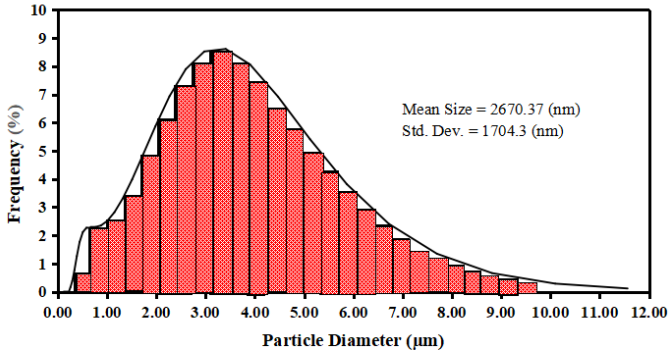

Fig. 4. Particle size of Fe_3O_4-TD using particle size analyzer (PSA Horiba LA 350)

Figure 4 presents the particle size of Fe_3O_4-TD. The average particle size of Fe_3O_4-TD was 2670.37 nm, much larger than the magnetic particle previously synthesized. The plant extract used in this study was tea dreg extract sourced from household waste. The content of active compounds in tea dregs extract was not as much as the content of active compounds in plant extracts or other wastes. The tea dregs have gone through the brewing stage causing many active compounds lost [20,28]. The active compounds in plants acted as capping agents that could control particle growth and prevent agglomeration during Fe_3O_4 synthesis.

Table 2. Comparison of the particle size of Fe_3O_4-TD with the crystal size of other magnetic particles

Plant extract	Synthesis condition	The average particle size (nm)
Leaf extract of *Zanthoxylum armatum* DC. [17]	pH 10, 60 min, 80°C	17
Seaweed (*Sargassum muticum*) Aqueous Extract [18]	60 min at 25°C	18.04
Archidendron pauciflorum peel extract (JPE) [8]	pH 11–12, 60 min, 60°C	318.3
Tea dregs extract (this study)	pH 11, 60 min, 60°C	2670.37

3.2. Effect of pH of MB solution on MB adsorption on Fe_3O_4-TD

It was prominent to study the effect of the pH of MB solution on MB adsorption on Fe_3O_4-TD because the surface sites of the adsorbent and adsorbate are affected by pH. In this study, the effect of the pH of MB solution on MB adsorption on Fe_3O_4-TD was studied in the range of 2-10. Based on Figure 5, the adsorption ability of MB adsorption on Fe_3O_4-TD at pH 4 was seen very good with % MB adsorption ~100%. The MB adsorption ability of Fe_3O_4-TD at pH = 2 was only about 48%. In this condition, the -OH groups on the surface of Fe_3O_4-TD were protonated to $-OH_2^+$. While, MB dyes were cationic at pH 2, so the electrostatic interactions were difficult. The surface condition of the protonated and deprotonated adsorbent was determined by pH_{zpc} Fe_3O_4-TD. In this study, the pHzpc Fe_3O_4-TD was not measured but based on previous studies, the pHzpc Fe_3O_4 synthesized without using plant extracts was in the range of pH 5-8, dependent upon the synthesis method [19,20].

The presence of organic compounds on the surface of Fe_3O_4 caused the pH_{zpc} Fe_3O_4 to decrease below pH 3 [19]. If the interaction between MB and Fe_3O_4-TD was through electrostatic interaction, then the adsorption ability of MB on Fe_3O_4-TD was lower below pH 3 and higher above pH 3. However, below pH 3, about 48% MB adsorbed on Fe_3O_4-TD. It was suspected that there was another interaction mechanism between MB and Fe_3O_4-TD. The alleged interaction was via hydrogen bonding and phi-phi interaction [2,20,21,27].

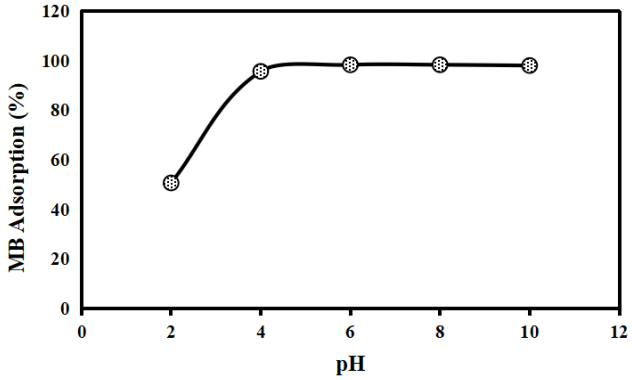

Fig. 5. Effect of pH of MB solution on MB adsorption on Fe_3O_4-TD

3.3. Effect of reaction time on MB adsorption on Fe_3O_4-TD

The variation of MB adsorption time on Fe_3O_4-TD was carried out to study the adsorption kinetics of MB on Fe_3O_4-TD. As shown in Figure 6, during the initial minutes of the reaction until the 15th minute, MB adsorption on Fe_3O_4-TD was very fast and continued to increase with time. In the early minutes, the surface of Fe_3O_4-TD was still not filled or not saturated, making it easier to interact with MB. After the 30th minute, the reaction rate slowed, and equilibrium reached the 90th minute. After 90 minutes, there was no increase in the percentage of MB adsorption on Fe_3O_4-TD because the surface of Fe_3O_4-TD was already saturated.

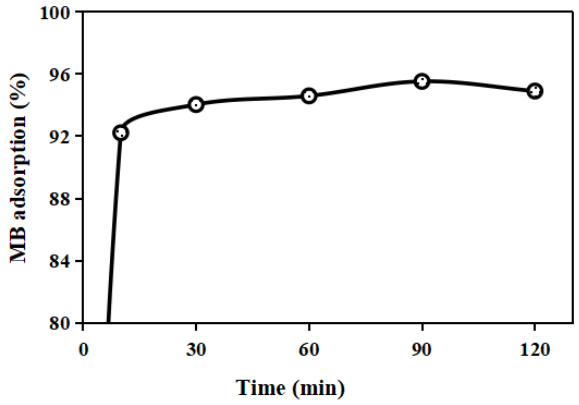

Fig. 6. Effect of reaction time of MB adsorption on Fe_3O_4-TD

3.4. Kinetic study of MB adsorption on Fe_3O_4-TD

The adsorption rate constant (k) is important in studying kinetics. It is a constant that is specific for each adsorption and has certain dimensions for each reaction order. The MB adsorption rate constant on Fe_3O_4-TD was determined using a kinetic model of pseudo-first-order Lagergren and pseudo-second-order Ho.

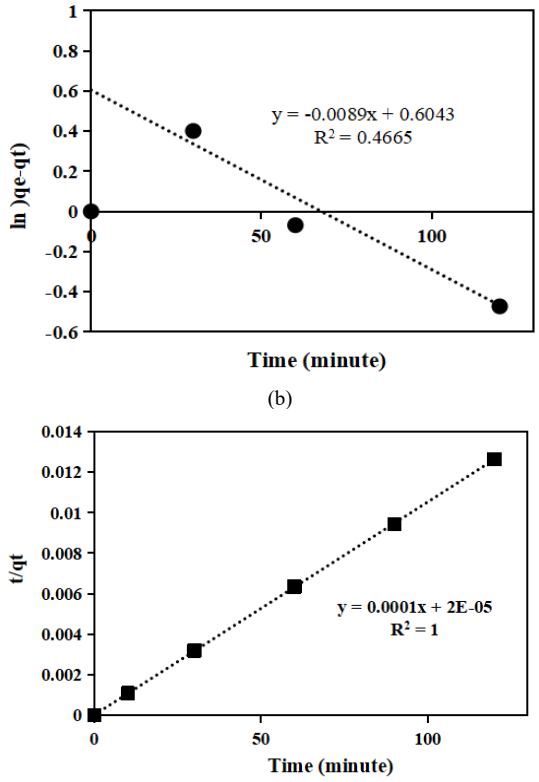

Fig. 7. Lagergren's pseudo first-order (a) and Ho's pseudo-second order (b) adsorption kinetics plots of methylene blue adsorption onto Fe_3O_4-TD

Lagergren pseudo-first-order kinetics model [22] MB adsorption on Fe_3O_4-TD was studied by making a linear graph of t against $\ln(q_e-q_t)$ based on equation (1). The graph shows the value of k (-slope) and q_e (calculated from the intercept). Figure 7 illustrates the first-order pseudo kinetics graph, according to Lagergren from the results of this study.

$$\ln(q_e - q_t) = -k_1 t + \ln q_e \quad (1)$$

The pseudo-second-order adsorption kinetics model proposed by Ho [23] was based on the adsorption capacity in the solid phase, as expressed by equation (2). From the graph between (t/q_t) vs t, it obtained the value of q_e (calculated, which was the amount of MB absorbed at equilibrium) and h (initial adsorption rate) resulting from the equation $h = kq_e^2$, so that the value of adsorption rate constant (k) obtained MB on Fe_3O_4-TD). The second-order pseudo kinetics graph, according to Ho from the results of this study, is presented in Figure 7.

$$\frac{t}{q_t} = \frac{1}{q_e} t + \frac{1}{k_2 q_e^2} \quad (2)$$

As shown in Figure 6, the R^2 value of the MB adsorption kinetics model curve on Fe_3O_4-TD, according to Lagergren's pseudo-first order, was very low, i.e. 0.4665. While the R^2 value of the pseudo-second-order kinetic model curve Ho was 1. These indicated that MB adsorption on Fe_3O_4-TD followed the pseudo-second-order Ho. The pseudo-second-order Ho model showed that the adsorption of MB on Fe_3O_4-TD involved two surface sites, and the solid capacity of Fe_3O_4-TD affected the adsorption process more than the concentration of MB solution. The interaction mechanism between MB and Fe_3O_4-TD occurred through chemosorption [24,25].

Meanwhile, Lagergren's pseudo-first-order kinetics model assumes that the concentration of the MB solution influences the adsorption process. This model is more suitable for the earliest step in the adsorption process because, at a later stage, there is a change in the concentration of the solution, which is directly proportional to the decrease in the number of available active sites, so this model is less applicable to MB adsorption on Fe_3O_4-TD [26]. When compared with previous studies with the same method [8], the initial adsorption rate of MB on Fe_3O_4-TD (tea dregs) was higher than the initial rate of MB adsorption on JMNPS (Jengkol peel). Likewise, the amount of MB absorbed in equilibrium at Fe_3O_4-TD (tea dregs) was higher than that of MB absorbed in equilibrium at JMNPS (jengkol peel). It was because the number of active sites in Fe_3O_4-TD (tea dregs) was fewer than the number of active sites in JMNPS (jengkol peel) in which the competition between active sites in interacting with MB was low.

3.5. Study of MB adsorption isotherm on Fe_3O_4-TD

The MB adsorption ability of Fe_3O_4-TD and the prediction of the interaction mechanism between MB and Fe_3O_4-TD can be studied through the adsorption isotherm model. The adsorption isotherm describes the relationship between MB in a given amount of Fe_3O_4-TD under equilibrium conditions and the initial concentration of MB in solution at a constant temperature. The adsorption isotherm models used in this study were the Freundlich isotherm and the Langmuir isotherm.

Langmuir isotherm assumes that the adsorption occurs in only one layer of adsorption (monolayer). If the adsorbate has covered the number of active sites on the adsorbent surface, the next adsorption process is hindered. Langmuir adsorption isotherm model is expressed by equation (3).

$$\frac{C_e}{q_e} = \frac{1}{q_{max} K_L} + \frac{C_e}{q_{max}} \quad (3)$$

The amount of MB adsorbed at equilibrium (mg g^{-1}) is expressed as qe, Ce is the concentration of MB in solution at equilibrium (mg L^{-1}), qmax is the maximum adsorption capacity (mg g^{-1}), and K_L is the Langmuir constant (L mol^{-1}), which corresponds to the adsorption energy. Based on equation 3, a straight line is obtained from the graph of Ce/qe against Ce. From the straight-line equation, the slope and intercept are obtained. The K_L value is 1/slope, while the intercept is $1/q_{max}$.

The Freundlich isotherm equation describes the non-ideal adsorption process on heterogeneous surfaces. Heterogeneity can be caused by differences in functional groups on the adsorbent surface. This isotherm model does not show the maximum amount of adsorption, so this model is suitable for the growth of an unlimited amount of adsorbed with increasing C_e concentration. Freundlich's isotherm model can be expressed by equation 4.

$$\log q_e = \log K_F + 1/n \log C_e \quad (4)$$

where q_e refers to the amount of MB adsorbed per gram of Fe_3O_4-TD at equilibrium (mg g^{-1}), C_e is the concentration of MB in solution at equilibrium (mg g^{-1}), K_F is the Freundlich constant associated with adsorption capacity, and 1/n is the heterogeneity factor. The values of K_F and n are obtained from the slope and intercept of the straight-line equation of the graph

of log q_e against log C_e. The value of n measures the deviation of adsorption from linearity.

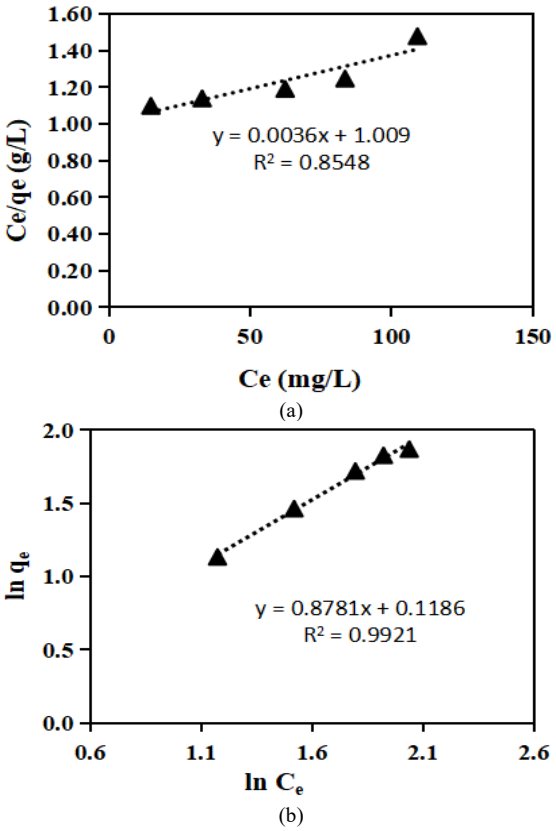

Fig. 8. Langmuir (a) and Freundlich (b) adsorption isotherms plots of methylene blue adsorption onto Fe_3O_4-TD

As seen in Figure 8 and the calculation results presented in Table 3, the MB adsorption isotherm on Fe_3O_4-TD followed the Freundlich adsorption isotherm model. It meant that the growth of MB adsorbed was not limited by the increasing concentration of C_e MB. MB adsorption on Fe_3O_4-TD was non-ideal adsorption on heterogeneous Fe_3O_4-TD surfaces. The surface heterogeneity of Fe_3O_4-TD was due to the organic compounds in tea dregs. Following the Freundlich adsorption isotherm model, the maximum adsorption capacity of MB on Fe_3O_4-TD could not be determined. From Table 4, the value of $1/n < 1$ indicated that the adsorption capacity of MB on Fe_3O_4-TD increased, and new adsorption sites were formed. It was the preferred adsorption model. These results were similar to previous studies using plant extracts in magnetite (Fe_3O_4) synthesis.

3.6. MB adsorption onto Fe_3O_4-TD mechanism

Based on the adsorption studies started from the effect of pH and kinetics studies to reveal the adsorption isotherms, Figure 9 presents the alleged interaction mechanism between MB and Fe_3O_4-TD. The most dominant interaction between MB and Fe_3O_4-TD was through electrostatic interactions. Above pH_{zpc} Fe_3O_4-TD (pH 3), MB adsorption on Fe_3O_4-TD was very good because, at this pH, the -OH group on the surface of Fe_3O_4-TD was deprotonated to $-O^-$, while MB was a cationic dye. The lower percent of MB adsorbed at pH below three was caused by the protonation of -OH group into $-OH^{2+}$, making it difficult for the the interaction between MB and Fe_3O_4-TD (Figure 5).

Based on the kinetics and adsorption isotherms studies, other alleged interactions occurred through hydrogen bonds and phi-phi interactions. Hydrogen bonding occurred between the H atom of the Fe_3O_4-TD active group molecule and the N atom of the MB molecule or between the O atoms of the Fe_3O_4-TD active group molecule and the H atom of the MB molecule. The phi-phi interaction was a non-covalent interaction that did not involve sharing electrons, so it was included in physisorption. It followed the adsorption isotherm model, namely the Freundlich isotherm model. The phi-phi interaction involved the delocalization of the plane charge distribution interactions of the conjugated aromatic ring on the Fe_3O_4-TD surface with the phi bonds on the MB aromatic ring.

The explanation of the MB adsorption mechanism on Fe_3O_4-TD was confirmed by post-adsorption FTIR spectra (Figure 10). No new absorption wave appeared, indicating the interaction between MB and Fe_3O_4-TD was not through a chemical interaction.

Table 3. Kinetic fits and parameters for MB adsorption

Adsorbent	Lagergren's pseudo first-order equation			Ho's pseudo first-order equation			
	R^2	q_e (mg/g)	k (minute^{-1})	R^2	q_e (mg/g)	h (mg/g.minute)	k (g/mg.minute)
Fe_3O_4-TD tea dregs (the current research)	0.4665	1.83	0.0089	1.0000	10000.0	50000	0.00050
JMNPS jengkol peel [3]	0.766	1.09	0.0143	0.9996	1428.6	2000	0.00098
Activated carbon derived from waste orange and lemon peels [29]	0.447	0.03	0.086	0.999	25.062	58.41	0.093
Humic acid [32]	0.912	11.139	0.020	0.980	11.139	-	0.002
Activated carbon of Coriandrum sativum [31]	0.913	62.677	0.037	1.000	79.365	-	7.94×10^{11}

Table 4. Isotherm fits and parameters for MB adsorption

Adsorbent	Langmuir parameters				Freundlich parameters		
	q_{max} (mol g^{-1})	K_L (L mol^{-1})	E_{ads} (kJ mol^{-1})	R^2	K_F (mol g^{-1})	n	R^2
Fe_3O_4-TD (tea dregs) this current research	0.00087	1141.19	17617.26	0.8548	10.21	1.14	0.9999
JMNPs (Jengkol peel) [3]	65.36	0.02	-10353.67	0.5345	9.08	1.15	0.9554
Activated carbon derived from waste orange and lemon peels [29]	33.0	1.00	-	0.9950	31.56	6.57	0.6480
activated Starbons® derived from starch [30]	-	-	-	-	632.30	16.34	0.9600
Activated carbon of Coriandrum sativum [31]	94.966	0.097	-	0.9890	16.62	3.004	0.9070
Humic acid [32]	66.225	0.034	-	0.9384	4.866	1.527	0.8431

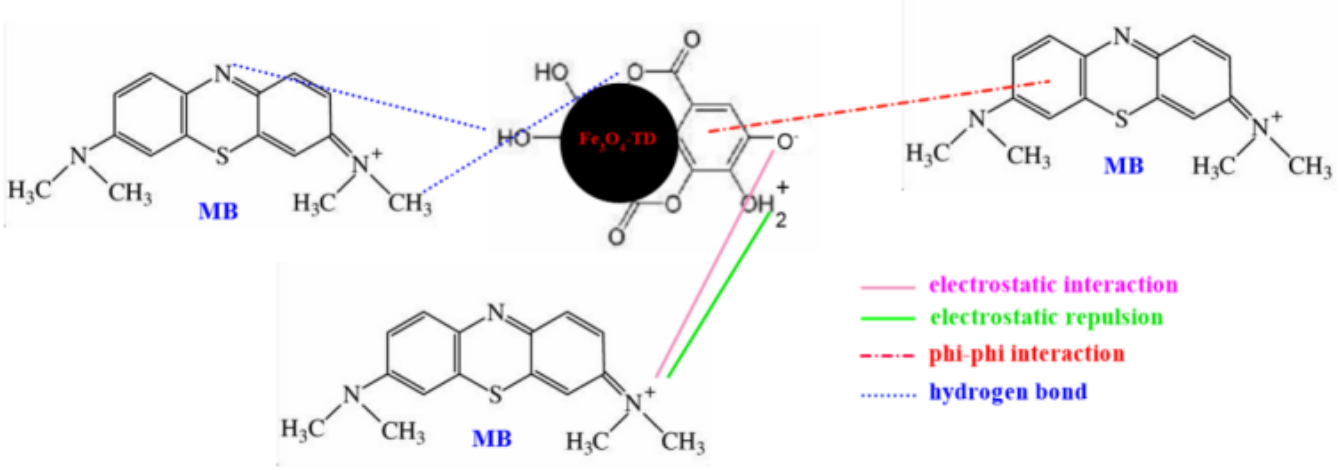

Fig. 9. Suggested mechanism for MB adsorption onto Fe_3O_4-TD

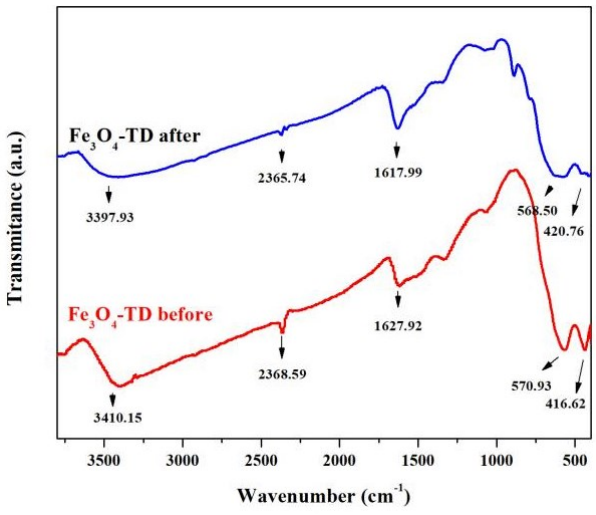

Fig. 10. FTIR spectra of Fe_3O_4-TD, before and after MB adsorption

4. Conclusion

Fe_3O_4-TD with good crystallinity has been successfully synthesized using tea dregs through co-precipitation method at room temperature. The particle size obtained was 26.70 µm. This result was found greater than the particle size of Fe_3O_4 from previous studies using fresh plant extracts. This difference might be due to the presence of active compounds in the tea dregs, reduced due to brewing for household consumption. However, the performance of Fe_3O_4-TD as an adsorbent for MB dye was very good. The adsorption capacity of MB on Fe_3O_4-TD was 10.21 mol/g. Interaction between MB Fe_3O_4-TD was through physisorption, allowing the adsorbent of Fe_3O_4-TD to be easily regenerated. It is necessary to do further research related to the reuse of Fe_3O_4-TD adsorbent.

Acknowledgement

The researcher would like to thank the Integrated Laboratory of UIN Sunan Kalijaga for the room facilities and equipment. The researcher also thanks the Chemistry Department of UIN Sunan Kalijaga Yogyakarta for the support provided.

References

1. M. Rahmayanti, E. Yunita, and N. F. Y. Putri. *Study of adsorption-desorption on batik industrial dyes (naphthol blue black) on magnetite modified humic acid (HA-Fe_3O_4)*. Jurnal Kimia Sains dan Aplikasi, 7

(2020) 244-248.

2. O. A. Saputra, Kurnia, S. Pujiasih, V. N. Rizki, B. Nurhayati, E. Pramono, C. Purnawan, *Silylated-montmorillonite as co-adsorbent of chitosan composites for methylene blue dye removal in aqueous solution*. Commun. Sci. Technol. 5 (2020) 45-52.
3. J. Shajeelammal, S. Mohammeda, K.P. Prathishc, A. Jeevae, A. Asok, and S. Shukla. *Treatment of real time textile effluent containing azo reactive dyes via ozonation, modifified pulsed low frequency ultrasound cavitation, and integrated reactor*. J. Hazard. Mater., (2022) 100098.
4. S. Ihaddadena, D. Aberkanea, A. Boukerrouia, and D. Robert. *Removal of methylene blue (basic dye) by coagulation-flocculation with biomaterials (bentonite and Opuntia ficus indica)*. JWPE, (2022) 102952.
5. W.M.A. El-Rahim, H. Moawad, A.Z.A. Azeiz, and M.J. Sadowsky. *Biodegradation of azo dyes by bacterial or fungal consortium and identifification of the biodegradation products*. Egypt. J. Aquat. Res., 3 (2021) 269–276.
6. M. Song, B. Mu, and Ru-Dan Huang. *Syntheses, structures, electrochemistry and catalytic oxidation degradation of organic dyes of two new coordination polymers derived from Cu(II) and Mn(II) and 1-(tetrazo-5-yl)-4-(triazo-1-yl)benzene.* J. Solid State Chem., (2017) 1-7.
7. Q. Chen, C. Peng, W. Liu, S. Ning, G. Hua, Z.K. Zhao, et al. *Oxidative coupling of kraft lignin mediated with hypervalent iodine reagent (III) for enhanced removal of dye in water*. Ind. Crops Prod., (2022) 114234.
8. M. Rahmayanti, A.N. Syakina, I. Fatimah, and T. Sulistyaningsih. *Green synthesis of magnetite nanoparticles using peel extract of jengkol (Archidendron pauciflorum) for methylene blue adsorption from aqueous media*. Chem. Phys. Lett., (2022) 139834.
9. R.M. Cornell and U. Schwertmann. *The iron oxides: structure, properties, reactions, occurrence and uses*. Germany and USA: Weinheim and New York (VCH Verlagsgeseiischaft mbH), (1996).
10. Y.P. Yew, K. Shameli, M. Miyake, N. Kuwano, N.B. Khairudin, S.E. Mohamad, et al. *Green synthesis of magnetite (Fe3O4) nanoparticles using seaweed (Kappaphycus alvarezii) extract*. Nanoscale Res. Lett., (2016) 276.
11. H. Rasoulzadeh, A. Mohseni-Bandpei, M. Hosseini, and M. Safari. *Mechanistic investigation of ciproflfloxacin recovery by magnetite–imprinted chitosan nanocomposite: isotherm, kinetic, thermodynamic and reusability studies*. Int. J. Biol. Macromol., (2019) 712–721.
12. A. Sebastian, A. Nangia, and M.N.V. Prasad. *Cadmium and sodium adsorption properties of magnetite nanoparticles synthesized from Hevea brasiliensis Muell. Arg. bark: relevance in amelioration of metal stress in rice*. J. Hazard. Mater., (2019) 261–271.
13. M. Rahmayanti, S.J. Santosa, and Sutarno. *Sonochemical co-precipitation synthesis of gallic acid-modified magnetite*. Adv. Mater. Res., (2015) 286-289.
14. M. Rahmayanti, S.J. Santosa, and Sutarno. *Mechanisms of gold recovery from aqueous solutions using gallic acid-modified magnetite particles synthesized via reverse co-precipitation method*. Int. J. Chemtech Res., 4 (2016) 446–452.
15. M. Rahmayanti, S.J. Santosa, and Sutarno. *Modified humic acid from peat soils with magnetite (HA-Fe_3O_4) by using sonochemical technology for gold recovery*. Jurnal Bahan Alam Terbarukan, 2 (2020) 81–87.
16. F. Azadia, A. Karimi-Jashnia, and M.M. Zerafat. *Green synthesis and optimization of nano-magnetite using Persicaria bistorta root extract and its application for rosewater distillation wastewater treatment*. Ecotoxicol. Environ. Saf., (2018) 467–475.
17. A. V. Ramesh, Dharmasoth Rama Devi, Satish Mohan Botsa, and K. Basavaiah. *Facile green synthesis of Fe_3O_4 nanoparticles using aqueous leaf extract of Zanthoxylum armatum DC. for efficient adsorption of methylene blue*. J. Asian Ceram. Soc., 2 (2018) 145-155.
18. Mahnaz Mahdavi, Farideh Namvar, Mansor Bin Ahmad, and Rosfarizan Mohamad. *Green biosynthesis and characterization of magnetic iron oxide (Fe_3O_4) nanoparticles using seaweed (Sargassum muticum) Aqueous Extract*. Molecules, 5 (2013) 5954-5964.
19. H. Luo, S. Zhanga, X. Li, X. Liu, Q. Xu, J. Liu, at al. Z. *Tannic acid modifified Fe_3O_4 core–shell nanoparticles for adsorption of Pb^{2+} and Hg^{2+}*, J. Taiwan Inst. Chem. Eng., (2017) 1–8.
20. Tayyebeh Madrakian, Abbas Afkhami, and Mazaher Ahmadi. *Adsorption and kinetic studies of seven different organic dyes onto magnetite nanoparticles loaded tea waste and removal of them from wastewater samples*. Spectrochim. Acta A Mol., (2012) 102–109.
21. M. Rahmayanti, I. Nurhikmah, and F. Larasati, F. *Isolation, characterization and application of humin from Sumatran peat soils as adsorbent for naphtol blue black and indigosol blue dyes*. Molekul, 1 (2021) 67–74.
22. S.K. Lagergren. *About the theory of so-called adsorption of soluble substances*. Sven. Vetenskapsakad. Handingarl, (1898) 1−39.
23. YS Ho, and G. McKay. *Pseudo-second order model for sorption processes*. Process Biochem., 5 (1999), 451−465.
24. M. Allaoui, M. Berradi, M., J. Bensalah, H. Es-sahbany, H., O. Dagdag, and S. Ibn Ahmed, S. *Study of the adsorption of nickel ions on the sea shells of Mehdia: kinetic and ther modynamic study and mathematical modelling of experimental data*. Materialsttoday: Proc., 8 (2021) 7494-7500.
25. Rayane de Oliveira Zonato, Bianca Ramos Estevam, Isadora Dias Perez, Valquíria Aparecida dos Santos Ribeiro, and Rosane Freire Boina. *Eggshell as an adsorbent for removing dyes and metallic ions in aqueous solutions*. CLCE, (2022) 100023.
26. José Helber VINCO, Amilton Barbosa BOTELHO JUNIOR, Heitor Augusto DUARTE, Denise Crocce Romano ESPINOSA, and Jorge Alberto Soares TENÓRIO. *Kinetic modeling of adsorption of vanadium and iron from acid solution through ion exchange resins*. Trans. Nonferrous Met. Soc. China, 7 (2022) 2438−2450.
27. M. El-Kammah, E. Elkhatib, S. Gouveia, C. Cameselle, and E. Aboukila. *Enhanced removal of indigo carmine dye from textile effluent using green cost-efficient nanomaterial: adsorption, kinetics, thermodynamics and mechanisms*. Sustain. Chem. Pharm., (2022), 100753.
28. N. Tekin, S.E. Karatay, G. Donmez. *Optimization studies about efficient biobutanol production from industrial tea waste by Clostridium beijerinckii*. Fuel, 331 (2023), 125763.
29. D. Ramutshatsha-Makhwedzha, A. Mavhungu, M. L. Moropeng, R. Mbaya. *Activated carbon derived from waste orange and lemon peels for the adsorption of methyl orange and methylene blue dyes from wastewater Heliyon*. 8 (2022) e09930.
30. H. Li, V.L. Budarin , J.H. Clark, M. North, X. Wu. *Rapid and efficient adsorption of methylene blue dye from aqueous solution by hierarchically porous, activated starbons®: Mechanism and porosity dependence*. J. Hazard. Mater.. 436 (2022), 129174.
31. C.C. Souza, L.Z.M. Souza, M. Yılmaz, M.A. Oliveira, A.C.S. Bezerra, E.F. Silva, M.R. Dumont, A.R.T. Machado, *Activated carbon of Coriandrum sativum for adsorption of methylene blue: Equilibrium and kinetic modeling*. Cleaner Materials. 3 (2022), 100052.
32. N. Ahmad, F. Suryani Arsyad, I. Royani, A. Lesbani, *Adsorption of methylene blue on magnetite humic acid: kinetic, isotherm, thermodynamic, and regeneration studies, Results in Chemistry*, (2022).